Soil Dynamics and Earthquake Engineering 116 (2019) 668–680

Contents lists available at ScienceDirect

Soil Dynamics and Earthquake Engineering

journal homepage: www.elsevier.com/locate/soildyn

The July 20, 2017 Bodrum-Kos, Aegean Sea Mw = 6.6 earthquake; preliminary field observations and image-based survey on a lateral spreading site

George Papathanassiou[a,*], Sotiris Valkaniotis[b], Spyros Pavlides[c]

[a] Department of Civil Engineering, Democritus University of Thrace, Greece
[b] Koronidos 9, 42100 Trikala, Greece
[c] Department of Geology, Aristotle University of Thessaloniki, Greece

ARTICLE INFO

Keywords:
Kos
Structure from motion
Lateral spreading
Liquefaction
Greece

ABSTRACT

The earthquake Mw6.6 (macroseismic intensity VIII, ESI-07 scale) that occurred on July 20, 2017 at 22:31 UTC (01:31 local time) in Gökova Bay, SE Aegean Sea, induced minor damages to contemporary structures at the island of Kos, Greece, while severe damages were reported on Venetian and Ottoman-era constructions, causing two deaths. Focusing on the island of Kos, secondary effects were reported in the eastern part, including liquefaction-related phenomena and tsunami. The generation of the latter one indicates the likelihood to this type of effects in the Aegean Sea. Liquefaction-induced lateral spreading caused severe structural damages at the waterfront area of the city of Kos. This area was investigated in detail few days after the event, by performing field measurements using a surveyor's tape and additionally, by applying SfM-based technique using a ground-based digital camera. The values of horizontal deformation, measured by these two techniques are in agreement, while on vertical axis a deviation of 12% is resulted.

1. Introduction

On July 20, 2017 at 22:31 UTC (01:31 local time) a shallow earthquake of Mw6.6 magnitude occurred in Gökova Bay at a depth of ≈10 km (Fig. 1). The epicenter of the earthquake, located between Bodrum, Turkey and the island of Kos, Greece, SE Aegean Sea. In particular, according to Kandilli Observatory and Earthquake Research Institute (KOERI) the epicenter was at 36.9620°N 27.4053°E, while according to the National Observatory of Athens (NOA) at 36.9643°N 27.4332°E. The fault plane strikes N280°E and dips to the north with an angle of about 40 degrees in a nearly E-W direction with surface deformation that reached about 20 cm onshore islet Karaada (Ganas et al. [1]). Preliminary inversion results of geodetic data, as constrained by InSAR observations, suggest that the upper edge of the fault (16 km length and 11 km width) is offshore (near the Gokova ridge bathymetric feature) at a very shallow depth (1 ± 0.5 km) (Ganas et al. [1]).

The recorded acceleration at the city of Bodrum, which is located at an epicentral distance of 12 km was 158.76 cm/sec.^{2}. Based on the preliminary distribution of peak ground acceleration (PGA), provided by ITSAK [2], the PGA values at the city of Kos and cape Louros were estimated as 0.2 g and 0.25 g, respectively (ITSAK [2]). It should be pointed out that Yasuda et al. [3] have shown that liquefaction phenomena were triggered by the 2003 Tokachi-oki earthquake in areas where the measured PGA values were equal to 0.05 g.

The primary goal of this study is to document the earthquake-induced secondary effects and to provide quantitative data regarding the characteristics of the liquefaction related phenomena at the island of Kos. In order to achieve this, a post-earthquake field survey was organized by the Department of Geology, Aristotle University of Thessaloniki on 13–14 August 2017.

Based on the field observations, it can be summarized that the earthquake caused damages to the building stock of the town of Kos, mainly to Ottoman and Venetian-era constructions, including partial collapses that killed two people and seriously injured several others. Damages were also reported in the city of Bodrum. Focusing on the island of Kos, the most remarkable type of environmental effects is the liquefaction related phenomena that induced severe damages to the port facilities and to the custom building at the new port of Kos, and at the old harbor of the city. Moderate liquefaction-induced structural failures were induced at the marina of Kos, while at cape Louros ejected material due to liquefaction covered more than 450 m^2. Furthermore, a tsunami wave was reported indicating that the generation of tsunami-

* Corresponding author.
E-mail address: gpapatha@civil.duth.gr (G. Papathanassiou).

https://doi.org/10.1016/j.soildyn.2018.10.038
Received 19 October 2017; Received in revised form 11 August 2018; Accepted 30 October 2018
0267-7261/ © 2018 Elsevier Ltd. All rights reserved.

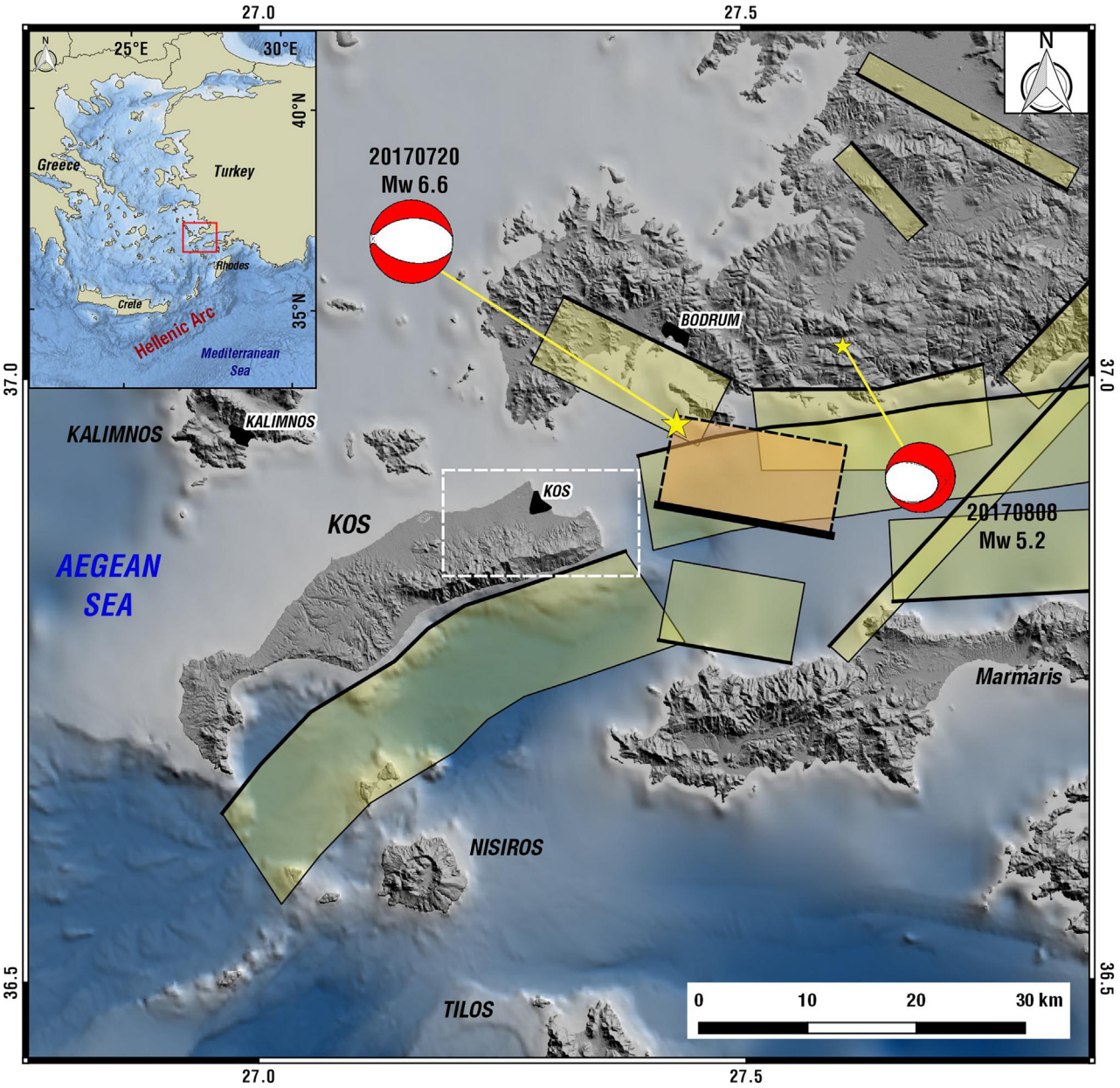

Fig. 1. The July 20, 2017 M_w 6.6 earthquake and the August 8, M_w 5.2 aftershock. Seismogenic sources and fault data from SHARE (Basili et al. [6]) and GreDAAS (Pavlides et al. [7]) databases. Revised epicenters and moment tensors from NOA. Orange box shows proposed preliminary fault plane from Ganas et al. [1]. The white box delineates the area shown in Fig. 2a (For interpretation of the references to color in this figure legend, the reader is referred to the web version of this article.).

related phenomena e.g. flooding and structural damages is likely in the Aegean Sea. In particular, the tsunami effects were observed at the south coast of Bodrum peninsula and at the northeast coast of Kos Island, with a maximum run-up measured at 1.9 m at Bodrum area (Yalçıner et al. [4]). Small-scale size rockfalls were reported in the southern part of the island of Kos.

Taking into account the quantitative characteristics of the earthquake-induced secondary effects e.g. liquefaction phenomena and tsunami, the macroseismic intensity was evaluated by applying the Environmental Seismic Intensity (ESI-07), a scale based only on environmental effects introduced by Michetti et al. [5]. Thus, the macroseismic intensities at the coastal area of cape Louros and the at waterfront area of the city of Kos were assessed as VIII taking into account i) the dimensions of liquefaction manifestations in the former case, ii) the lateral spreading and subsidence at the port and at the old harbor of the city of Kos, and iii) the characteristics of the generated tsunami documented by Yalciner et al. [4]. Details regarding the liquefaction related phenomena are presented in Sections 5.1 and 5.2 in this article.

The secondary goal of this study is to investigate in detail a lateral spreading site, located at the old harbor of the city of Kos. This was achieved by performing traditional ground measurements as well as an image-based survey following the Structure from Motion (SfM) technique in order to virtually measure the deformation. The novelty of this study is related to the fact that the applied SfM technique for measuring the lateral spreading displacement was based on a simple ground-based digital camera instead of a UAV.

2. Historical seismicity on the island of Kos

The island of Kos can be considered as an area of moderate seismicity taking into account the information provided by published seismic catalogues. In particular, according to Ambraseys and Finkel

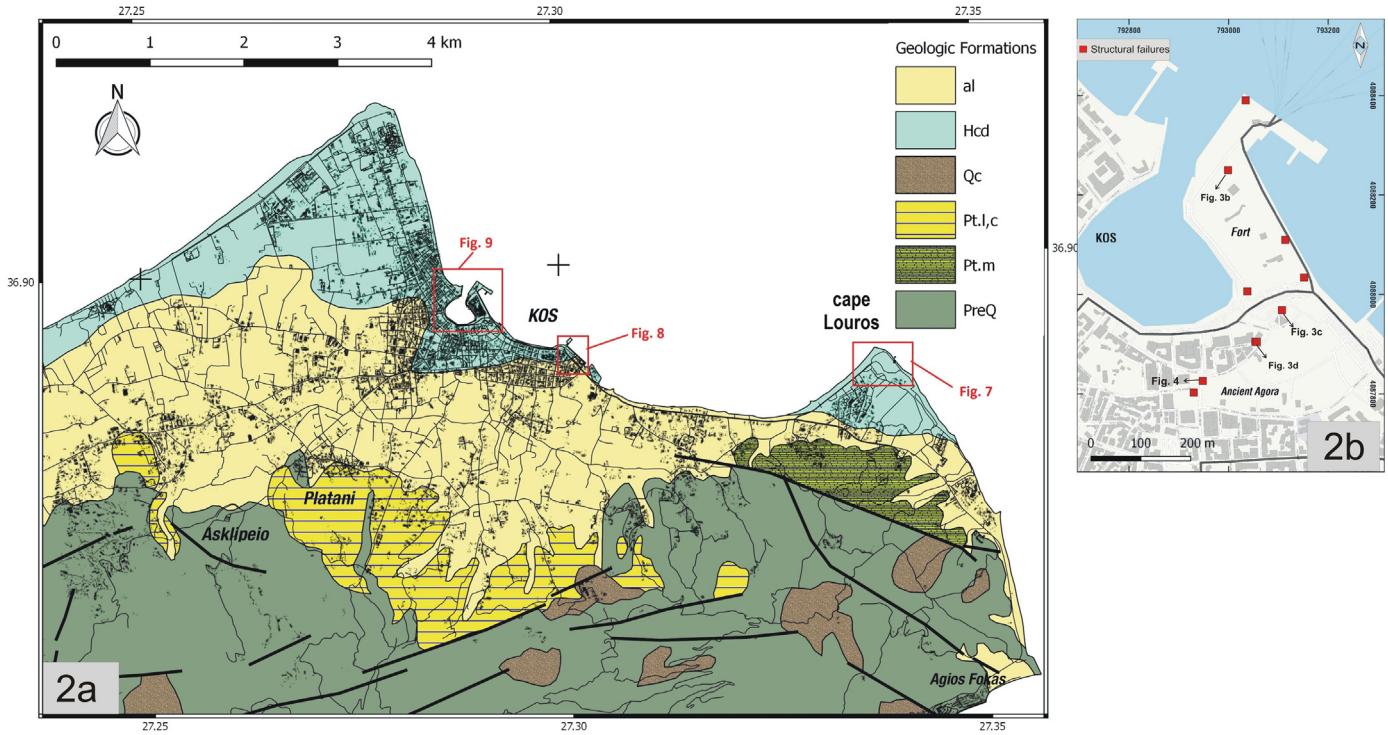

Fig. 2. a. Map of Quaternary sediments in the eastern Kos area; al: Alluvial deposits, Hcd: Coastal & lagoonal deposits, Qc: Quaternary scree and debris, Pt.l,c: Pleistocene lacustrine and terrestrial deposits, Pt.m: Pleistocene marine deposits, PreQ: Pre-Quaternary formations (Geologic data modified from Triantafyllis [22]). Fig. 2b. Locations of structural failures induced by the 2017 earthquake at the city of Kos.

[8], Papazachos and Papazachou [9], Guidoboni et al. [10], Guidoboni and Comastri [11] and Ambraseys [12], the most well documented events are the ones occurred on August 18, 1493 and April 23, 1933. The latter earthquake caused 200 deaths, while the city of Kos was totally destroyed. According to Papazachos and Papazachou [9], in many places the ground sunk by one meter; a subsidence that could be related to liquefaction-induced failures assuming that these sites are located at the waterfront area. This event also induced structural damages at Bodrum. The *October 18, 1493* event (MM IX; Guidoboni et al. [10]) induced severe damages to the houses as well as to the walls and to the fortress at the city of Kos, and at the fortified settlements of Andimakhia, Pylion and Kefalos. According to the description provided by Guidoboni and Comastri [11], there were many deaths and injuries, while this event may be responsible for the collapse of the mausoleum of Halicarnassus (present-day Bodrum). According to Ambraseys [12], coastal buildings collapsed and fell into the sea.

Much less information is available regarding the failures induced by the events occurred on 412 BCE (MM IX), 334 (MM VIII), 459 (MM IX), and 556 (MM X), and 1673; the values of macroseismic intensity MM are provided by Papazachos and Papazachou [9]. In particular, the first event that occurred on **412 BCE**, induced the collapse of the fortress of the city according to Thucydides (Papazachos and Papazachou [9]), while on **334 AC** many structures collapsed due to the earthquake (Guidoboni et al. [10]; Papazachos and Papazachou [9]). The **459** earthquake completely destroyed the island of Kos (Papazachos and Papazachou [9]) and the **556** event, triggered a phenomenon that could be related to tsunami since according to Guidoboni et al. [10] and Papazachos and Papazachou [9] the sea rose up and engulfed all the buildings near the shore, destroying them. According to Ambraseys and Finkel [8], the **1673** earthquake is related to the event that gives rise to the myth about the island of Kos being swallowed up. It should be pointed out that this event is not listed on the earthquake catalogue published by Papazachos and Papazachou [9].

Thus, it could be preliminary concluded that similar secondary effects as the ones triggered by the July 20, 2017 earthquake, e.g. liquefaction–related phenomena and tsunami, may had been triggered by historical earthquakes at the city of Kos and particularly, by the 1933 and the 556 events, respectively.

3. Geology – tectonics

The island of Kos is situated in the southeastern part of the Aegean Sea, close to the Minor Asia mainland. The island is part of the South Aegean Volcanic Arc complex, with volcanic deposits of Miocene to Pleistocene age and a system of SW-NE to W-E offshore disrupted by the Kefalos and Nisyros volcanic complexes (Nomikou et al. [13]; Papanikolaou and Nomikou [14]). The easternmost part of Kos island defines the borders of the major Gökova Gulf graben of Plio-Quaternary age. This extensional graben is defined by a complex pattern of mainly extensional fault with a mainly W-E strike mapped along the coast and offshore (Kurt et al. [15]; Uluğ et al. [16]; İşcan et al. [17]; Tur et al. [18]). Major faults onshore Kos island with a WSW-ENE strike follow the bedrock mountain range in the south part of Island and the uplifted Neogene sediments on the north. A younger set of brittle detachment faults in the foothills south of Kos city is believed to be related with post-orogenic collapse after the Miocene (van Hinsbergen and Boekhout [19]).

The coastal eastern part of Kos island consists of a broad strip of Holocene coastal and lagoonal deposits (sands, silt and gravel), and an alluvial plain of sand, gravel, conglomerates and clay deposits (Fig. 2a). Quaternary scree and debris are mapped to the southern part of the island. Pleistocene shallow marine to terrestrial deposits can be found at the hills located to the south and east of the city of Kos. They consist of a variety of conglomerates, tuffs, terrace deposits, sands, sandstones, marls and marly limestones (Altherr et al. [20]; Willmann [21]; Triantafyllis [22]).

Pre-Quaternary formations mapped to the south of Kos city consist of Permo-Carboniferous anchimetamorphic sediments exposed at the Dikeos tectonic window, upper Mesozoic and lower Cenozoic carbonate units and Palaeogene wildflysch with olistoliths. These bedrock

Fig. 3. A) Pre-earthquake photo of the site (photo uploaded by Sofia Karagianni on 24 March 2012, on Panoramio Google earth), b) Horizontal movement of the statue parallel to the direction of the shaking, c) One of the two fountains of the Gazi Hasan Pasha Mosque, located at the old part of the city of Kos, was completely collapsed d) heavily damaged building at the old part of the city of Kos (photographs b,c and d taken by G. Papathanassiou on August 14, 2017).

formations were intruded by the Kos monzonite around 12 Ma (Altherr et al. [20]; van Hinsbergen and Boekhout [19]). Miocene to Pleiocene shallow marine and lacustrine sediment unconformably overly the Alpine formations in the northern foothills.

4. Geological and structural failures induced by the July 20, 2017 earthquake

One of the most characteristic effects triggered by the 2017 earthquake was the tsunami that affected the coast of Bodrum and the northeast coast of the island of Kos. In particular, according to Yalciner et al. [4] the tsunami-related main effects were localized in Gumbet Bay, Bodrum Peninsula, Turkey. The maximum run-up of about 1.9 m was observed at the mouth of a small dry stream, while no damage happened in the next bay (Bitez bay at West and Bodrum marina at East of Gumbet bay). The sea receded 5 min after the earthquake and advanced up to 60 m inundation at 13th minute with run-up traces at 2 m elevation at Karaada-Black Island (Yalciner et al. [4]). In the area of the island of Kos, the height of tsunami was les than 1 m and reported in the coast outside the city and in the old harbor of the city (Yalciner et al. [4]). The reader is referred to the report of Yalciner et al. [4] for more information regarding the generation and the consequences of the

Fig. 4. A) Pre-earthquake photo of the arch (photo taken on October 20, 2015 and uploaded by Kos tourism on Panoramio, Google earth), b) post-earthquake photo showing the downward movement of the keystone (yellow color) (photo taken by G. Papathanassiou on August 14, 2017) (For interpretation of the references to color in this figure legend, the reader is referred to the web version of this article.).

tsunami.

Regarding the earthquake-induced failures to the manmade environment, minor damages were observed on contemporary residential houses and buildings that were constructed following the regulations of the Greek Seismic Code. However, severe damages have been observed on constructions of Ottoman and Venetian-era. The locations of these failures are shown in Fig. 2b. In particular, the castle of Nerantzia, built by the knights of St John in the mid-14th century at the entrance of the old harbor on the eastern part of the city, was seriously damaged and a crack of 10 cm opening was reported in the northwestern wall. At the same area, which is located between the western side of the castle and the heavily damaged custom building, a lateral shifting of a statue towards the west was documented. The direction of the movement is parallel to the direction of the causative fault (Fig. 3a and b).

At the area of castle, we have been informed that a mixture of soil and water was ejected through an abandoned well, and that the ejected grey material covered the area around it (M. Lefatzis and M. Chalkiti personal communication). Opposite the castle of Nerantzia at Lotzia Square, near the “tree of Hippocrates”, the Gazin Hasan Pasan Mosque that was built in 1786 was heavily damaged (Fig. 3c) and the local authorities forbade the public entrance. In addition, two people killed when an Ottoman-era house partially collapsed (Fig. 3d).

Moreover, at the centre of the old city of Kos and particularly, at the Kazouli Square the Deftedar mosque and the Ancient gate to Roman Agora were damaged. In the latter case, the downward movement of the keystone in the arch (Fig. 4b) is considered as a typical earthquake effect on archeological sites. In particular, according to Kamai and Hatzor [23], this type of secondary effect can be induced only by major earthquakes ($M > 6.5$), and is usually developed due to a decreasing load to the walls of the arches. Furthermore, the occurrence of the downward sliding of the keystone is related to the seismic shock direction. In particular, Rodríguez-Pascua et al. [24] stated that this sliding can be developed only when the angle formed by the seismic direction and the arch is smaller than 45°. However, this conclusion is not in agreement with this case study (Bodrum/Kos 2017 event), since the relevant angle is much larger than 45°. This case of earthquake archeological effect (EAE) will be further analyzed in near future when quantitative data will be available. The reader is referred to the article of Rodríguez-Pascua et al. [24] for more information regarding the usefulness and analyses of the EAE in seismic hazard analysis.

Regarding the generated secondary ruptures/cracks on the island of Kos, it was feasible to map them at the eastern part of the island close to cape Louros (location is shown in Fig. 2a). In particular, a crack on the paved road of an average width of 3 cm was observed. Along this direction at a distance of few meters to the west, the pavement was cracked and two distinct segments were formed. As it is shown in Fig. 5b, the inner part overimposed upon the outer one creating a “step” of 10 cm vertical displacement that resulted to the closure of the entrance of the nearby hotel.

Finally, small-scale size rock falls were observed at one site at the southern part of the island. These phenomena did not cause any structural damages or disruption of the road traffic and were immediately removed by local authorities.

5. Liquefaction – related phenomena in the island of Kos

The most remarkable secondary effects triggered by the July 20, 2017 earthquake are the liquefaction related phenomena. These phenomena were reported in the eastern part of the island, and particularly at cape Louros (10 km epicentral distance) and at the waterfront area of the city of Kos (12 km epicentral distance). In the former case, we were able to map liquefaction manifestations that did not induce any structural failures, while on the latter one, lateral spreading caused severe damages at the port facilities e.g. quays, sidewalks and piers, and at the old harbor of Kos. It should be pointed out that similar phenomena with the ones reported in the waterfront area of the city of Kos are frequently documented on structures located on relevant areas worldwide.

Having mapped the liquefaction occurrences, a back analysis was

Fig. 5. A) Pre-earthquake photo of the entrance (©2017 Google earth), b) post-earthquake cracks at the same location (photos taken by G. Papathanassiou on August 13, 2017).

performed in order to assess liquefaction susceptibility at these sites. This preliminary type of analysis, which is commonly applied in liquefaction studies, is based on the correlation of the epicentral distance of the liquefaction manifestations with the earthquake magnitude. In this study, we employed the seismic parameters (magnitude M and epicenter's coordinates) as they were defined both by KOERI and NOA, and we took into consideration the published regressions proposed by Ambraseys [25], Papadopoulos and Lefkopoulos [26], Aydan et al. [27], and Papathanassiou et al. [28]. The regression published by Ambraseys [25] was developed based on worldwide data, while the other three regressions have been developed by taking into account data provided by historical liquefaction occurrences documented at this tectonic regimen e.g. Greece and Turkey. As it is shown in Fig. 6, the liquefaction phenomena triggered by the Bodrum/Kos 2017 earthquake, documented during the field survey e.g. “liquefied sites”, fall within the distance commonly defined as ‘liquefiable zone’ (to the left of the curves). The outcome arising from Fig. 6 is that the published curves are still valid, and accordingly they can be used for a preliminary screening of liquefaction susceptibility.

5.1. Liquefaction-induced failures at cape Louros

At the area of cape Louros, three zones of liquefaction manifestations have been documented. The area is preliminary characterized as very likely to liquefaction since according to the geological map (Fig. 2a), is covered by Holocene age coastal and lagoonal deposits.

In particular, the grey material that was ejected through ground cracks covered more than 450 m^2 (Fig. 7). During the post-earthquake reconnaissance field survey, we used the “track” function in a GPS handle unit in order to accurately map the liquefied zones and document their dimensions; area (m^2), perimeter (m) and centroid per zone (Table 1). In particular, we used the GIS kit app (© 2017 Garafa, LLC) and the Bad elf GPS for lightning connector for iPad 2. The web tool used for the accomplishment of this goal is the one developed for the purposes of LAMPRE Project (http://www.lampre-project.eu/), aiming to document landslides. As it is presented in this study, this tool can additionally be used for mapping areas covered by liquefied material.

At the liquefied zone 1, a ground crack of 2 m length, 50 cm width and 40 cm depth was documented through which grey color mixture of soil and water was ejected and covered 142 m^2 (Fig. 7e). The perimeter of the covered area is 57 m and the centroid of the area is on 36.8892938°, 27.3375461°. At zone 2, the mixture of soil and water was ejected through a sand crater of 12 cm diameter and a nearby ground crack with dimensions of 24 cm width, 50 cm length and 11 cm depth, and covered 208 m^2 (Fig. 7c). The perimeter of the area is 64 m with centroid on 36.8902587°, 27.3382231°. At the third zone, the liquefied material was ejected through a crack of 80 cm width, 90 cm length and 55 cm depth (Fig. 7d). The ejecta covered 139 m^2 and the perimeter of the area is 77 m with centroid on 36.8900282°, 27.3377017°. Soil samples from these three liquefied zones were collected and analyzed in the laboratory of Engineering Geology and Hydrogeology of Aristotle University of Thessaloniki; the results are presented in Section 5.3. At the same location, a subsidence of the coastal area was documented. The post-earthquake position of the lighthouse, which was initially constructed 10 m far from the coastline, is now practically standing on it due to subsidence and the inundation of the coast (Fig. 7b). At the same area, two craters of an average of 50 cm diameter were reported without any evidence of liquefaction origin ejecta.

5.2. Liquefaction related phenomena at the waterfront area of the city of Kos

The marina of the island of Kos was constructed on 2001 and is located at a distance of 1 km to the east of the capital of Kos. At this area, extremely large amount of brown material was ejected through cracks of up to 8 cm width on the pavement aprons (Fig. 8). The ejecta covered almost all the area that is used as a dry dock and for the maintenance and repairs of sailboats and yachts (Fig. 8c, d and e). Furthermore, the liquefaction of the subsoil induced failures to the lifelines; according to a witness the pipelines were broken. One sample was collected from the ejecta and analyzed, showing that the dominant particle size of the material is sand. In addition, the earthquake induced structural failures at the main area of marina and particularly, cracks of 4–5 cm width were observed on the sidewalk with direction parallel to the seashore. At the main pier, cracks on the pavement aprons with horizontal and vertical displacement were documented and an area of approximately 30 m^2 covered by ejected material (Fig. 8a). It must be pointed out that these cracks were not parallel to the seashore. At the same area, at pier F, a system of cracks on the pavement induced a subsidence of the site forming a "graben" (Fig. 8b).

The most severe liquefaction-induced failures were reported in the waterfront area of the city of Kos and particularly, in the old harbor and in the newly constructed port area (Fig. 9). The mechanism of the failure was similar to the one described by Cubrinovski et al. [29]; large ground shaking first displacing the retaining structure outwards (e.g. towards the sea), which is then followed by lateral spreading in the backfills.

In particular, parallel cracks on the pier of 10–15 cm width that were developed due to lateral spreading phenomena, resulting to the totally loss of functionality of the port and of the custom building (Fig. 9a and b). Walking parallel to the seashore towards the lighthouse, a crack of 100 m length was reported behind the quay wall. The horizontal and vertical displacement along this crack varied with

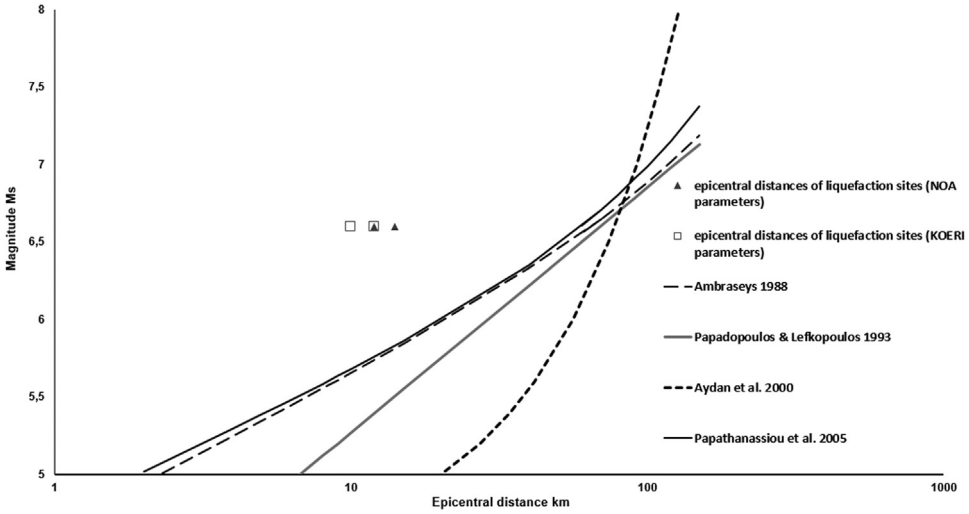

Fig. 6. Distribution of the liquefied sites and comparison to the proposed upper bound curves for the assessment of liquefaction susceptibility.

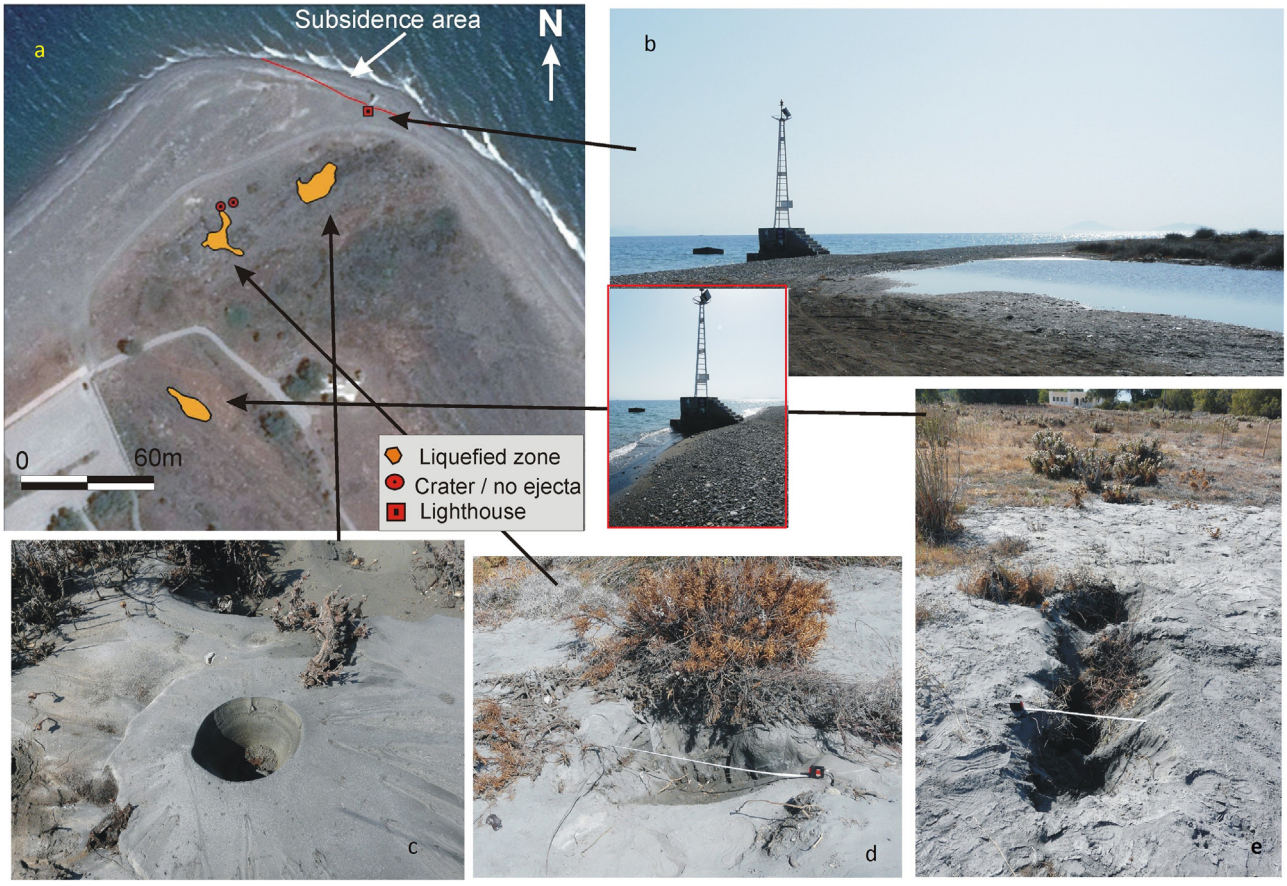

Fig. 7. Earthquake-induced ground failures at the cape Louros (all photos taken by G. Papathanassiou on August 13, 2017). A) Plan view of the area (background image from ©2017 Google earth) showing the location of the reported secondary effects, b) subsidence and inundation of the coast at the area of the lighthouse, c) sand crater at the liquefied zone 2, d) ground crack through which liquefied material was ejected at the liquefied zone 3, e) ground crack through which liquefied material was ejected at the liquefied zone 1.

Table 1
Dimensions of the liquefied zones documented at the area of cape Louros.

Liquefied zone	Area (m^2)	Perimeter (m)	Centroid
1	142	57	36.8892938°, 27.3375461°.
2	208	64	36.8902587°, 27.3382231°
3	139	77	36.8900282°, 27.3377017°

maximum subsidence of 35 cm at the edge of the pier. At this site, a tilting of 6 degrees of the lighthouse was measured (Fig. 9g). A perpendicular crack to the seashore on the pavement aprons and the parallel to the seashore crack, formed a graben-like phenomenon at the main dock of the port.

At the old harbor of the city, which nowadays is used by both tourist vessels as well as ferries, cracks parallels to the seashore were

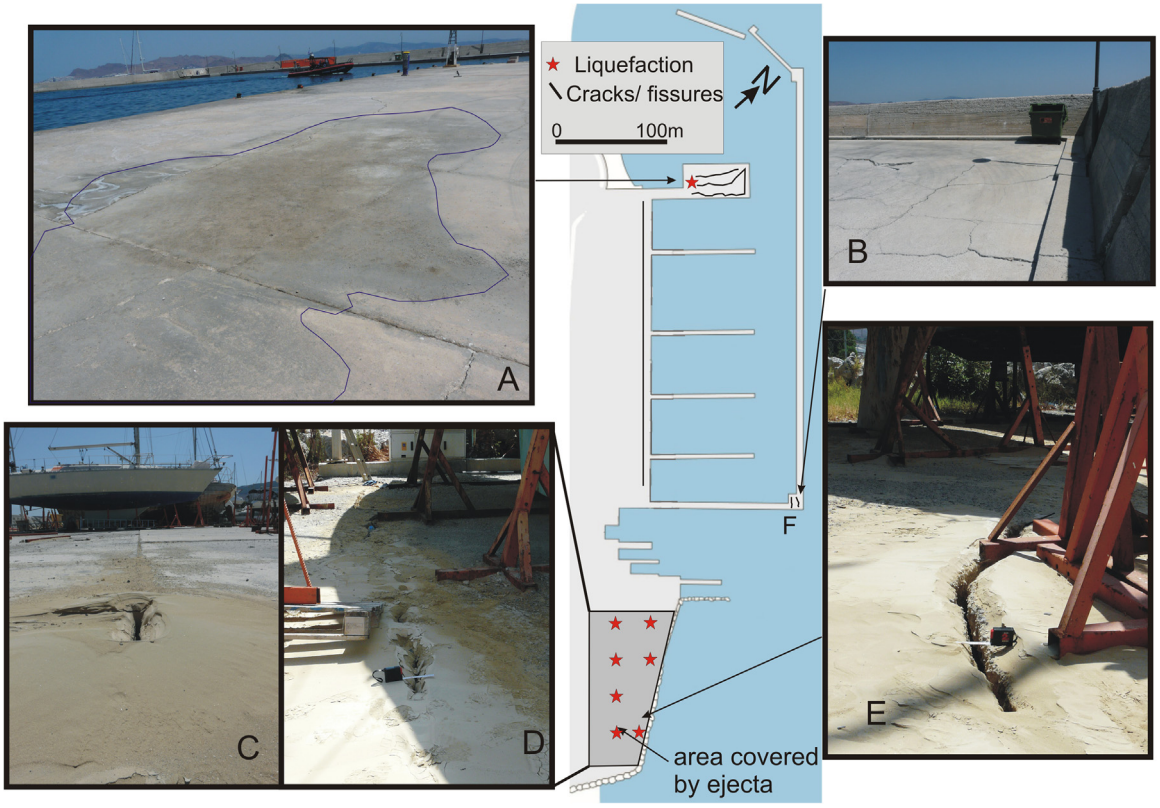

Fig. 8. Liquefaction-induced failures documented at the area of marina (all photos taken by G. Papathanassiou on August 13, 2017), a) ejected material at the main pier, b) cracks at pier F, and c,d,e) liquefaction manifestations at the area of marina that is used as a dry dock and for the maintenance and repairs of sailboats and yachts.

documented. In particular, a fissure of up to 5 cm wide on the sidewalk and a parallel crack behind the quay wall with horizontal displacement of up to 10 cm and up to 35 cm vertical offset, induced severe subsidence (Fig. 9c). Moving towards the castle, the cracks were extended to the nearby park where lateral spreading phenomena were observed in a distance of 12 m from the seashore (Fig. 9d and e). This area was studied in detail and the results are presented in the Section 5.4.

5.3. Grain size analysis of ejecta

During the field survey, four (4) samples of ejected material were collected and analyzed at the Laboratory of Engineering Geology and Hydrogeology of the Department of Geology at the Aristotle University of Thessaloniki in order to define their grain size characteristics. All the samples of the ejected materials are classified as sandy ones with low percentage of fines (< 10%). In particular, the first sample (1st) that was collected on the liquefied zone 1 (Fig. 7e) is classified as sand with 3.4% fines. The second sample (2nd), collected on the liquefied zone 2 (Fig. 7c), is characterized as sand with 4.2% fine particles, while the third one (Fig. 7d) was collected on the liquefied zone 3 and is also characterized as sand with 5.1% fines. The grain size analysis of the brown ejected material that was collected on the area of marina of Kos indicates a sandy material with fines content 8.5%. That material was probably used as a fill beneath the pavement aprons.

Taking into account that the 1st, 2nd and 3rd sample were collected from the same area (cape Louros) and that their gradation is similar based on the conducted grain size analysis, it was decided to plot in Fig. 10 only one gradation curve with red solid color e.g. 2nd sample, in order to facilitate the reader. The 4th sample that collected at the area of marina is represented by a blue dashed line. As it is shown in Fig. 10, the particle size distribution curves of the collected samples are in the range of likely to liquefaction soils, defined by Tsuchida [30].

5.4. Lateral spreading measurements based on manually and image-based techniques

The July 20, 2017 earthquake triggered “typical” lateral spreading phenomena both at the piers of the main port as well as at the old harbor of the city of Kos. The latter case was investigated in detail by conducting manually and virtual measurements following a photogrammetric survey.

Structure from motion (SfM) photogrammetry can be performed with images acquired by consumer-grade digital cameras (Eltner et al. [31]). Usually, a photogrammetric survey is based on Unmanned Aerial Vehicles UAV that uses flexible multicopters equipped with webcams, digital cameras and other various sensors (Eltner et al. [31]; Colomina and Molina [32]; Lidner et al. [33]). This approach is considered as a cost-effective and efficient means to acquire dense and accurate data of earth surface (Lucieer et al. [34]). Hence, it was followed by many researchers the last 5 years, mainly aiming to document landslides (Niethammer et al. [35]; Stumpf et al. [36]; Turner et al. [37]). Regarding liquefaction-induced lateral spreading phenomena, the UAV-based approach was performed by Franke et al. [38] during a reconnaissance field survey. However, using a UAV was not feasible in our case, and hence it was decided to perform a survey based on a hand-held digital camera in order to collect high-definition images. Thus, this study can be considered as the first one documenting lateral spreading phenomena by applying the Structure from Motion (SfM) technique using a simple commercial digital camera.

In particular, 70 images of the displacement area were captured along a straight line that was perpendicular to the seashore and parallel to the direction of the spreading, in order to produce a SfM point cloud using Agisoft Photoscan. The camera that was used on this post-earthquake reconnaissance survey was a Panasonic Lumix DMC-FZ18 of 8.1 megapixel resolution with an optical image stabilizer in the lens in

Fig. 9. Liquefaction related phenomena at the waterfront area of the city of Kos (all photos taken by G. Papathanassiou on August 14, 2017). A and B) lateral spreading phenomena induced damages to custom building, c) subsidence behind the quay wall at the old harbor, d,e) lateral spreading phenomena at the old harbor, f) failure at the new port of Kos, g) subsidence of 35 cm behind the quay wall at the main pier and tilting of 6° of the lighthouse. Background image of the plan view from © 2017 Google earth.

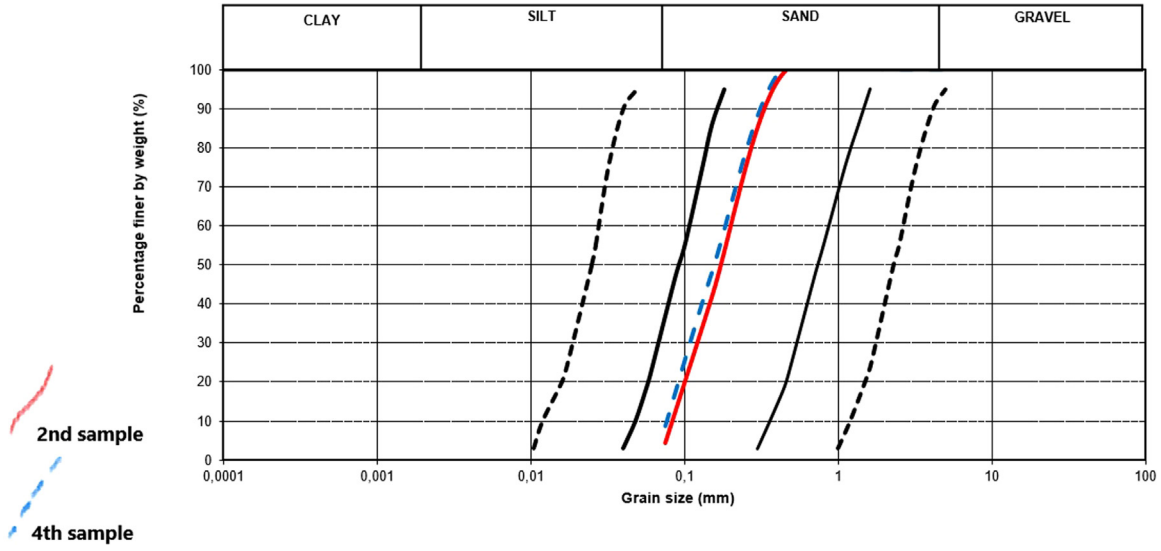

Fig. 10. Grain size analysis of the collected samples and comparison with boundary lines proposed by Tsuchida [30]. Red solid line represents the gradation curve of the 2nd sample and the blue dashed line shows the grain size distribution of the 4th sample. Solid black lines delineate the likely to liquefaction area, and the dashed black lines delineate the possible to liquefaction one (For interpretation of the references to color in this figure legend, the reader is referred to the web version of this article.).

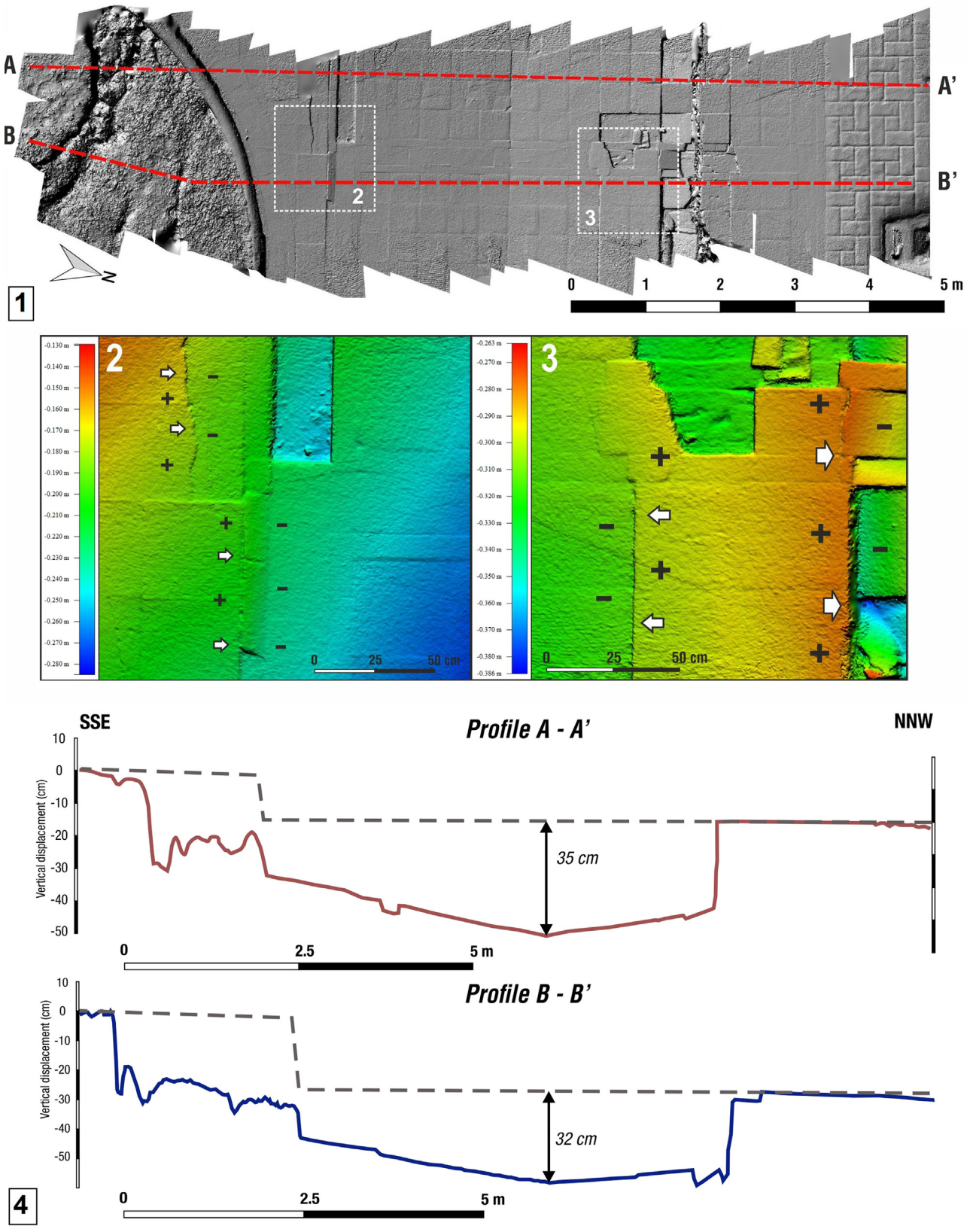

Fig. 11. 1. Shaded relief of digital surface model (0.3 cm pixel) extracted from the point cloud 2 and 3) Details from the digital surface model showing minor deformation structures and cracks (arrows). 4) Profiles showing complex vertical displacement along the lateral spreading feature. Dashed lines represents pre-earthquake surface. Maximum vertical deformation is calculated by the profiles at −35 and −32 cm.

Table 2
Measurements of horizontal and vertical displacement based on traditional field survey and Structure from Motion (SfM) technique (Profile A-A′ in Fig. 11). The starting point of the transect is on the coastline.

Manually			**SfM** (Profile A-A′)			
Distance (m)	Displacement (m)	Cumulative	Distance (m)	Displacement (m)	Cumulative	*Difference (m)*
Horizontal displacement (m)						
3.1	0.08	0.08	3.1	0.1	0.1	0.02
4.23	0.0135	0.0935	4.3	0.0145	0.1145	0.001
5.44	0.01	0.1035	5.63	0.02	0.1345	0.01
7.9	0.2	0.3035	8.27	0.21	0.3445	0.01
10.05	0.18	0.4835	10.2	0.14	0.4845	−0.04
10.27	0.62	1.1035	10.38	0.63	1.1145	0.01
					Median	**0.01**
Vertical displacement (m)						
3.1	0.3	0.3	3.1	0.28	0.28	0.28
4.23	0.01	0.31	4.3	0.015	0.295	0.015
5.44	0	0.31	5.63	0.03	0.325	0.03
7.9	0	0.31	8.27	0.017	0.342	0.017
10.05	0	0.31	10.2	0.05	0.392	0.05
10.27	0.3	0.61	10.29	0.3	0.692	0.3
					Median	**0.04**

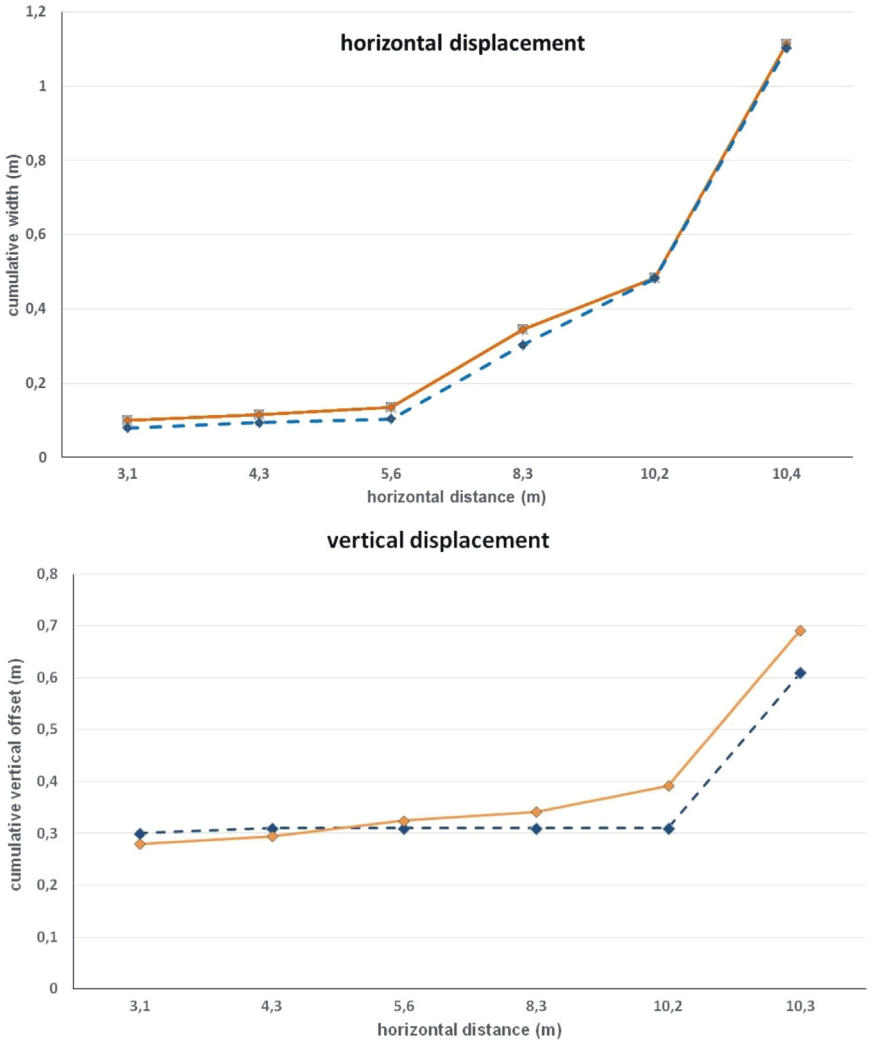

Fig. 12. Comparison of the cumulative horizontal displacements measured during the field survey (blue dashed line) with the ones provided by the SfM-based 3D point cloud (orange solid line), Profile A-A′ in Fig. 11. Top) horizontal displacement, bottom) vertical displacement (For interpretation of the references to color in this figure legend, the reader is referred to the web version of this article.).

order to reduce blurring by compensating for hand shake. Initial camera alignment was assisted by camera sensor GPS info and produced the original tie point set.

For the purposes of this survey, no ground control points were taken into account. Due to time restrictions, the point cloud product was georeferenced using points measured by a decimetric scale tape measure in order to define a local grid. As it is stated by Warrick et al. [39], these type of "control points", along with GPS information saved for each photo, may ensure adequate precision in the final point cloud. Using the optimize camera alignment command after the input of ground control points measured, initial alignment and tie points were corrected. The final point cloud was extracted by dense matching using ultra-high settings, in order to achieve the best resolution possible. Afterwards, a Digital Surface Model (DSM) and orthomosaic were exported based on the dense point cloud. The resulted digital surface model has a pixel size of 3 mm.

The traditional manual field survey was based on ground measurement technique performed along the same transect, following the procedure suggested by Ishihara et al. [40] and applied by Robinson et al. [41] and Cubrinovski et al. [29] in Christchurch, New Zealand and Franke et al. [38] in Iquique, Chile. In particular, along the line followed for the SfM-technique, the horizontal displacement (width of the cracks) and the vertical offset were measured at each location of failure (subsidence, cracks) using a surveyor's tape.

The outcome of SfM approach is shown in Fig. 11. In particular, initially a shaded relief of digital elevation model (0.3 cm pixel) was extracted from the point cloud dataset. In order to measure the maximum vertical offset, the point cloud obtained from the photogrammetric survey, was compared with a pre-earthquake ground surface profile. The latter one was reconstructed by taking into account pre-earthquake images of the specific location and descriptions provided by local authorities. As it is shown in Fig. 11, the maximum earthquake-induced vertical displacement is 35 cm, and was documented behind the quay wall.

Furthermore, having developed the 3D point cloud, we were able to measure the cumulative width of cracks and the vertical displacements following the photogrammetric technique at Profile A-A′ (Fig. 11). After that, the SfM measurements were compared with the ones obtained by the traditional field survey i.e. manual measurements. In particular, the distributions of the lateral spread displacements that were measured by these two techniques are listed in Table 2 and shown in Fig. 12. The cumulative width of the cracks, measured based on SfM technique, is 1.1145 m, and fits very well to the one measured by the traditional technique e.g. 1.1035 m (Fig. 12a); less than 1% deviation. The deviation for the cumulative vertical offset is approximately 12%, which can be considered as significant. It must be highlighted that this value is mainly resulted from the measurements for horizontal distance of greater than 8 m (Fig. 12b). In particular, as it is presented on Table 2, the vertical displacement measured based on SfM technique at 8 and 10 m distance from the seashore is 0.017 and 0.05 m respectively. At the same distances, no displacement was identified on the field during the traditional survey and consequently the relevant values are zero for both locations. As a result, the cumulative offset measured based on SfM is 0.692 m, while the one measured using a surveyor's tape on the field is 0.61 m (Fig. 12b).

6. Conclusions

The goal of this study was to document the secondary effects at the island of Kos and to describe in a quantitative way the liquefaction-induced failures triggered by the July 20, 2017 earthquake, by providing information regarding their characteristics e.g. width and length. In addition, samples of ejected material were collected and analyzed in the laboratory in order to define their grain size characteristics. The results of this analysis confirmed the boundary lines of likely and possible to liquefaction areas, based on the soil gradation, as they have been proposed by Tsuchida [30].

The majority of the documented liquefaction related failures was located at the waterfront area of the city of Kos. In particular, the new port and the custom buildings were strongly affected, resulting to the loss of their functionality. At the main pier, a subsidence of up to 35 cm and tilting of the lighthouse were documented. Cracks parallels to the seashore were reported in the old harbor of the city behind the quay wall with horizontal displacement up to 10 cm and up to 35 cm vertical offset. Liquefaction manifestations were reported in cape Louros, an area covered by Holocene age coastal deposits.

The second goal of this study was to measure on both axes the deformation induced by lateral spreading at the old port of Kos. This was achieved by applying SfM technique as well as traditional methods i.e. surveyor's tap, during field survey. Comparing the obtained measurements by these two methods, it is resulted that the deviation of the measurements on horizontal axis e.g. width of cracks, between the virtual (SfM-based) and the manually field observations is less than 1%. Thus, it can be concluded that the SfM-based technique provide reliable data regarding the lateral displacement and accordingly, could be used for the purposes of a rapid post-earthquake field survey. This technique can be appropriately applied even with a low cost ground-based technique e.g. a simple commercial digital camera. However, the outcome arisen from the comparison of the measurements on vertical axis cannot be characterized as satisfied, since a 12% deviation exists. Thus, it is highlighted that some caution should be applied when using this technique in order to measure the vertical offset. Finally, we would like to point out that this study is considered as a preliminary test regarding this approach and more tests should be applied in order to evaluate the capabilities of this technology.

Acknowledgements

We would like to thank the editor and the two anonymous reviewers for their comprehensive comments that helped improve this manuscript significantly. We additionally would like to thank M. Lefatzis and M. Chalkiti, for the information regarding the liquefaction related phenomena within the castle of the city of Kos and P. Kapiris and Ath. Tsapelis for their help during the field survey.

References

[1] Ganas A, Elias P, Valkaniotis S, Briole P, Kapetanidis V, Kassaras I, Barberopoulou A, Argyrakis P, Chouliaras G, Moshou A. Co-seismic deformation and preliminary fault model of the July 20, 2017 M6.6 Kos earthquake, Aegean Sea. 〈https://www.emsc-csem.org/Files/event/606346/Kos_report_30-7-2017.pdf〉 ; 2017.

[2] ITΣAK. Earthquake Mw6.6 July 21, preliminary report, ITSAK, OASP. Thessaloniki, 20 pages (in Greek); 2017. 〈http://www.itsak.gr/uploads/news/earthquake_reports/EQ_COS_20170721_M6.6.pdf〉.

[3] Yasuda S, Morimoto I, Kiku H, Tanaka T. Reconnaissance report on the damage caused by the three Japanese earthquakes in 2003. In: proceedings of the 11th ICSDEE and 3rd ICEGE. Berkeley CA USA; vol. 1. 2004. p.14–21.

[4] Yalçıner A, Annunziato A, Papadopoulos G, Dogan G, Guler H, Cakir T, Sozdinler C, Ulutas E, Arikawa T, Suzen L, Kanoglu I, Guler I, Probst P, Synolakis C. The 20th July (22:31UTC) Bodrum/Kos earthquake and Tsunami, post tsunami field survey report. 2017; 2017. 〈http://users.metu.edu.tr/yalciner/july-21-2017-tsunami-report/Report-Field-Survey-of-July-20-2017-Bodrum-Kos-Tsunami.pdf〉.

[5] Michetti AM, Esposito E, Guerrieri L, Porfido S, Serva L, Tatevossian R, Vittori E, Audemard F, Azuma T, Clague J, Comerci V, Gurpinar A, McCalpin J, Mohammadioun B, Mörner NA, Ota Y, Roghozin E. Intensity Scale ESI 2007. Mem. Descr. Carta Geol d'Italia. 74, Rome; 2007.

[6] [database] Basili R, Kastelic V, Demircioglu MB, Garcia D, Nemser ES, Petricca P, Sboras SP, Besana-Ostman GM, Cabral J, Camelbeeck T, Caputo R, Danciu L, Domac H, Fonseca J, García-Mayordomo J, Giardini D, Glavatovic B, Gulen L, Ince Y, Pavlides S, Sesetyan K, Tarabusi G, Tiberti, MM, Utkucu M, Valensise G, Vanneste K, Vilanova S, Wössner J. The European database of seismogenic faults (EDSF) compiled in the framework of the Project SHARE; 2013. 〈http://diss.rm.ingv.it/share-edsf/〉. 〈http://dx.doi.org/10.6092/INGV.IT-SHARE-EDSF〉.

[7] Pavlides S, Caputo R, Sboras S, Chatzipetros A, Papathanasiou G, Valkaniotis S. The Greek catalogue of active faults and database of seismogenic sources. Bull Geol Soc Greece 2010;43(1):486–94.

[8] Ambraseys NN, FInkel CF. The seismicity of Turkey and adjacent areas. A historical review, 1500-1800. EREN 1995. p. 240–1995.

[9] Papazachos B, Papazachou C. The earthquakes of Greece. Thessaloniki: Ziti Publ.;

1997. p. 304.
[10] Guidoboni E, Comastri A, Raina GT. Catalogue of the ancient earthquakes in the mediterranean area up to the 10th century. Bologna: ING, Roma-SGA; 1994. p. 504.
[11] Guidoboni E, Comastri A. Catalogue of earthquakes and tsunamis in the Mediterranean area, 11th-15th century. Rome: Instituto Nazionale di Geofisica e Vulcanologia; 2005.
[12] Ambraseys N. Earthquakes in the mediterranean and middle east: a multi-disciplinary study of seismicity up to 1900. Cambridge University Press; 2009.
[13] Nomikou P, Papanikolaou D, Alexandri S, Ballas D. New insights on the Kos–Nisyros volcanic field from the morphotectonic analysis of the swath bathymetric map. Rapp Comm Int Mer Medit 2004:37–60.
[14] Papanikolaou D, Nomikou P. Tectonic structure and volcanic centres at the eastern edge of the Aegean Volcanic arc around Nisyros island. Bull Geol Soc Greece 2001;34(1):289–96.
[15] Kurt H, Demirbağ E, Kuşçu İ. Investigation of the submarine active tectonism in the Gulf of Gökova, southwest Anatolia–southeast Aegean Sea, by multi-channel seismic reflection data. Tectonophysics 1999;305:477–96.
[16] Uluğ A, Duman M, Ersoy Ş, Özel E, Avcı M. Late quaternary sea-level change, sedimentation and neotectonics of the Gulf of Gökova: Southeastern Aegean Sea. Mar Geol 2005;221:381–95.
[17] İşcan Y, Tur H, Gökaşan E. Morphologic and seismic features of the Gulf of Gökova, SWAnatolia: evidence of strike-slip faulting with compression in the Aegean extensional regime. Geo-Mar Lett 2013;33(1):31–48.
[18] Tur H, Yaltirak C, Elitez I, Sarıkavak K. Pliocene-quaternary tectonic evolution of the Gulf of Gökova, southwest Turkey. Tectonophysics 2015;638:158–76. https://doi.org/10.1016/j.tecto.2014.11.008.
[19] Van Hinsbergen DJJ, Boekhout F. Neogene brittle detachment faulting on Kos (E Greece): implications for a southern break-away fault of the Menderes metamorphic core complex (western Turkey) 311. Geol Soc. London Special Publications; 2009. p. 311–20. https://doi.org/10.1144/SP311.12.
[20] Altherr R, Keller J, Kott K. Der jungtertiare Monzonit von Kos und sein Kontakthof (Agais, Griechenland). Bull Soc Geol Fr 1976;18:403–12.
[21] Willmann R. Neogen und jungtertiare Enwicklung der Insel Kos (Agais, Griechenland). Geol Rundsch 1983;72:815–60.
[22] Triantafyllis M. Geological Map of Greece in scale 1:50.000, West and East Kos Island Map Sheets. Institute for Geological and Mineralogical Exploration, Athens; 1989.
[23] Kamai R, Hatzor YH. Numerical analysis of block displacements in ancient masonry structures: a new method to estimate historic ground motions. Int J Numer Anal Methods Geomech 2007;32:1321–40.
[24] Rodríguez-Pascua MA, Pérez-López R, Giner-Robles JL, Silva PG, Garduño-Monroy V, Reicherter K. A comprehensive classification of earthquake archaeological effects (EAE) in archaeoseismology: application to ancient remains of Roman and Mesoamerican culture. Quat Int 2011;242:20–30.
[25] Ambraseys NN. Engineering seismology. Int J Earthq Eng Struct Dyn 1988;17:1–105.
[26] Papadopoulos AG, Lefkopoulos G. Magnitude – distance relation for liquefaction in soil from earthquakes. Bull Seismol Soc Am 1993;83(3):925–38.
[27] Aydan O, Ulusay R, Kumsar H, Tuncay E. Site investigation and engineering evaluation of the Duzce-Bolu earthquake of November 12, 1999. Turkish Earthquake Foundation, Instanbul. Report No. TDV/DR 09-51; 2000. p. 307.
[28] Papathanassiou G, Pavlides S, Christaras B, Pitilakis K. Liquefaction case histories and empirical relations of earthquake magnitude versus distance from the broader Aegean region. J Geodyn 2005;40(2–3):257–78.
[29] Cubrinovski M, Robinson K, Taylor M, Hughes M, Orense R. Lateral spreading and its impacts in urban areas in the 2010–2011 Christchurch earthquakes, New Zealand. J Geol Geophys. 2012;55(3):255–69.
[30] Tsuchida H. Estimation of liquefaction potential of sandy soils. In: Proceedings of the 3rd joint meeting, US-Japan, UNJR; 1971.
[31] Eltner A, Kaiser A, Castillo C, Rock G, Neugirg F, Abellan A. Image-based surface reconstruction in geomorphometry- merits, limits and developments. Earth Surf Dyn 2016;4:359–89.
[32] Colomina I, Molina P. Unmanned aerial systems for photogrammetry and remote sensing: a review. ISPRS J Photogramm Remote Sens 2014;92:79–97.
[33] Lindner G, Schraml K, Mansberger R, Hübl J. UAV monitoring and documentation of a large landslide. Appl Geomat 2016;8(1):1–11.
[34] Lucieer A, Turner D, King D, Robinson S. Using an unmanned (UAV) to capture microtopography of Antarctic moss beds. Int J Appl Earth Obs Geoinf 2013;27:53–62.
[35] Niethammer U, James M, Rothmund S, Travelletti J, Joswig M. UAV-based remote sensing of the Super-Sauze landslide: evaluation and results. Eng Geol 2012;128:2–11.
[36] Stumpf A, Malet J-P, Kerle N, Niethammer U, Rothmund S. Image-based mapping of surface fissures for the investigation of landslide dynamics. Geomorphology 2013;186:12–27.
[37] Turner D, Lucieer A, Jong SM. Time series analysis of landslide dynamics using an unmanned aerial vehicle (UAV). Remote Sens 2015;7:1736–57.
[38] Franke K, Rollins K, Ledezma C, Hedengren J, Wolfe D, Ruggles S, Bender C, Reimschiissel B. Reconnaissance of two liquefaction sites using small unmanned aerial vehicles and structure from motion computer vision following the April 1, 2014 Chile earthquake. J Geotech Geoenviron Eng 2016;V143(5). [04016125-1-11].
[39] Warrick JA, Ritchie AC, Adelman G, Adelmann K, Limber PW. New techniques to measure cliff change from historical oblique photographs and structure-from-motion photogrammetry. J Coast Res 2017;33:39–55.
[40] Ishihara K, Yoshida K, Kato M. Characteristics of lateral spreading in liquefied deposits during the 1995 Hanshin-Awaji earthquake. J Earthq Eng 1997;1(1):23–55.
[41] Robinson K, Cubrinovski M, Kailey P, Orense R. Field measurements of lateral spreading following the 2010 Darfield earthquake. In: Proceedings of the 9th Pacific conference on earthquake engineering, 14–16 April, Auckland 2011 paper no. 52: 1–8; 2010.